NAS5-29279

IN-74
64274

PHOTOELECTROCHEMICAL FABRICATION OF SPECTROSCOPIC DIFFRACTION GRATINGS

FINAL REPORT
SBIR Phase I Research

for Period February 13, 1986 - August 12, 1986

CONTRACT NO. NAS5-29279

EIC Laboratories, Inc.
111 Downey Street
Norwood, Massachusetts 02062

Prepared for

NASA Goddard Space Flight Center
Greenbelt, Maryland 20771

September, 1986

NOTICE--SBIR DATA--PHASE I

This SBIR data is furnished under NASA Contract No. NAS5-29279. It is furnished in confidence with the understanding that it will not, without permission of the contractor, be used for other than Governmental purposes nor disclosed outside the Government except for evaluation for Phase II selection purposes and under an understanding of confidentiality with the evaluator; provided however, in the event a Phase II contract is awarded as a follow-on to this Phase I contract, the Government may obtain additional rights to use and disclose this data. This Notice shall be affixed to any reproduction of this data, in whole or in part.

ACKNOWLEDGMENTS

The following staff members at EIC Laboratories contributed to this project: Dr. R. David Rauh (Principal Investigator), Dr. Michael M. Carrabba, and Ms. Nguyet M. Nguyen. We would also like to acknowledge the very helpful discussions with Dr. Anthony Caruso and Dr. Bruce E. Woodgate of the NASA Goddard Space Flight Center. This work was partially supported by the Office of Naval Research.

TABLE OF CONTENTS

LIST OF ILLUSTRATIONS

LIST OF ILLUSTRATIONS - cont'd

PROJECT SUMMARY

Photoelectrochemical etching has been demonstrated as a means of fabricating a variety of periodic structures in semiconductors. The semiconductor is used as an electrode in an electrochemical cell, and is in contact with a liquid electrolyte. When the crystal is held at a positive voltage and illuminated, etching occurs in only the illuminated regions to a depth proportional to the illumination intensity and exposure time. In Phase I it was determined that diffraction gratings could be produced in gallium arsenide crystals by this method, using either a scanned focused laser beam or by uniform illumination of a ruling mask defined in metal or photoresist on the crystal surface. The latter approach was determined to produce V-grooves if the mask is oriented along certain crystallographic directions. These V-grooves have been produced with an exceedingly smooth crystal morphology due to the highly controllable nature of the process and the very mild electrolytes involved (e.g., 1M KCl). The results form the basis for photoelectrochemical fabrication of deep, low pitch Eschelle gratings for use in high orders in NASA spectroscopic instrumentation such as the Space Telescope Imaging Spectrograph (STIS).

1.0 INTRODUCTION

Diffraction gratings are critical components in many of NASA's space missions for the purpose of spectral analysis of light from stellar and albedo sources and as optical reflectors, beam splitters and filters. For example, the space telescope contains a faint object spectrograph and camera, and a high resolution spectrograph, each utilizing spectroscopic gratings. Missions such as Spacelab, infrared and x-ray astronomical observatories and the Extreme Ultraviolet Explorer all rely on spectrographic dispersive components to gain information about the composition of the universe.

Diffraction gratings are extremely sensitive optical components which require much care and precision in manufacture. Furthermore, in the space environment they can undergo thermal stresses and be subjected to radiational and particulate fluxes not found on earth. Most gratings manufactured for terrestrial spectroscopy are fabricated from organic polymer, either as holographically exposed photoresist or as epoxy-based replicas of masters. In general, polymers leave much to be desired with respect to mechanical hardness and thermally induced volume changes, which are factors even when metallic thin film reflecting overcoating is applied. Masters are generally ruled in soft metal films on optically flat glass substrates. Masters can be produced in a limited number of soft materials (e.g., Al, Au), and have several drawbacks. The ruling process is very slow, because of the number of grooves required for a grating of practical size and mechanical/vibrational limitations to the rate of diamond scribing each groove with a ruling engine. The material displacement, imperfect ruling engines, and difficulty in maintaining precise environmental control and vibration isolation over the long times required to complete a ruling (often 1-2 weeks) all give rise to ultimate limitations in quality and production costs.

Two particularly difficult structures to produce are Eschelle gratings and transmission gratings (1). Eschelle gratings have deep, triangular grooves, but have a low pitch and thus are used in high orders. Transmission gratings are always replicas of ruled masters, and are thus limited to organic resins. Because these are refractive rather than reflective dispersive elements, they are limited by the optical homogeneity of the resin material, and are generally of lower optical quality than reflection gratings. Nevertheless, they would provide simplified mountings in many space applications if quality could be assured.

Obviously one would like to manufacture gratings over a wide range of pitches and a variety of groove profiles in materials suitable to the space environment. To this end, we proposed in Phase I to examine photoelectrochemical etching of diffraction gratings. This process would enable production of a range of groove profiles directly in hard inorganic materials. Using this method, interferometric gratings can be produced in many semiconductor materials (e.g., Si, Ge, ZnSe, CdS, ZnO, $BaTiO_3$) (2-4,6). These

materials could be used as substrates for reflection gratings, or even as transmission gratings in the energy region below their optical bandgaps. Indeed, any optically projected image can be etched into the semiconductor surface. The semiconductor can be either a single crystal or a thin film deposited on (e.g.) optically flat glass, mylar, etc.

In the photoelectrochemical method, the grating is etched into the surface of a semiconductor with n-type doping. The semiconductor is mounted in an electrochemical cell containing an electrolyte, and its potential controlled versus a reference electrode using a potentiostat. As shown in Figure 1, at positive potentials a space charge region develops at the semiconductor-electrolyte interface, with associated upward bending of the conduction and valence bands. When the semiconductor is irradiated with light of energy greater than its bandgap, holes (minority carriers) are produced in the valence band which diffuse to the surface under the internal field. For most semiconductors in most aqueous electrolytes, these holes are sufficiently energetic to decompose the crystal lattice, giving rise to oxidation products (5). Modulated by the photon flux, etching will occur at the illuminated surface if the products are soluble in the electrolyte.

Several arrangements for photoelectrochemical etching of grating structures are shown in Figure 2. The regions to be etched can be exposed using a mask comprised of photoresist or other material. Single step etching techniques are also possible, i.e., projecting an image of the grating profile onto the crystal surface, or using a scanned focused laser to induce localized photoelectrochemical etching. The extent of etching can be monitored as the photocurrent, while the rate can be controlled via the light intensity and applied potential. It is a particular advantage of photoelectrochemical processing that the high degree of process control means that precise conditions can be maintained to ensure uniformity and smoothness of etched features.

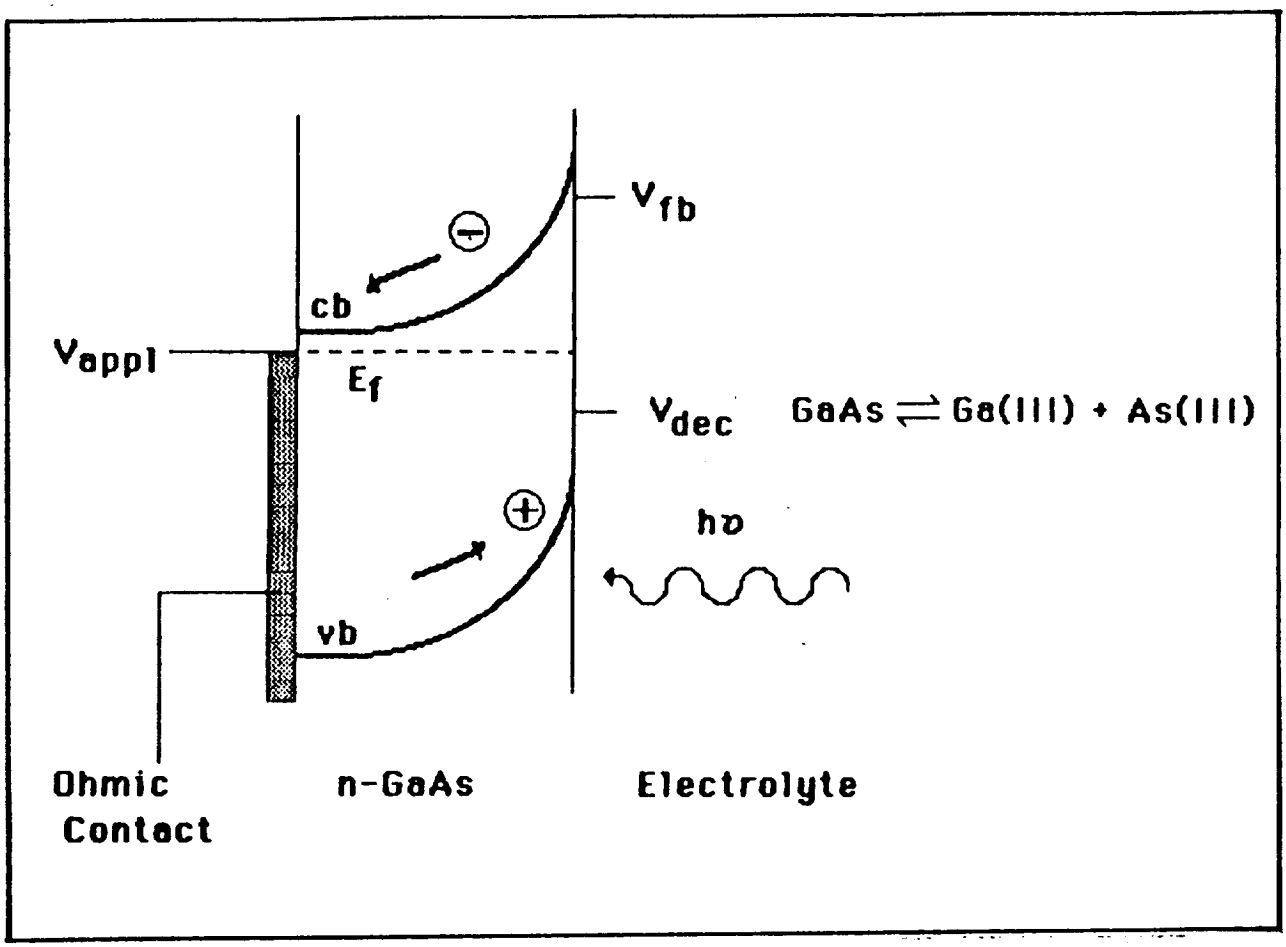

Figure 1. Energy diagram showing the band bending at the n-GaAs/electrolyte interface (cb = conduction band, vb = valence band, E_f = Fermi level). The bands are unbent (by definition) when the applied potential, V_{appl}, equals the flat band potential, V_{fb}. Increased bending occurs when V_{appl} becomes more positive, leading to increased efficiency of separation of electrons and holes. The width of the band bending region (W) should be greater than the light penetration depth for efficient separation of photon generated electrons and holes. Also shown is the anodic decomposition potential of GaAs, V_{dec}.

PHOTOELECTROCHEMICAL IMAGING TECHNIQUES

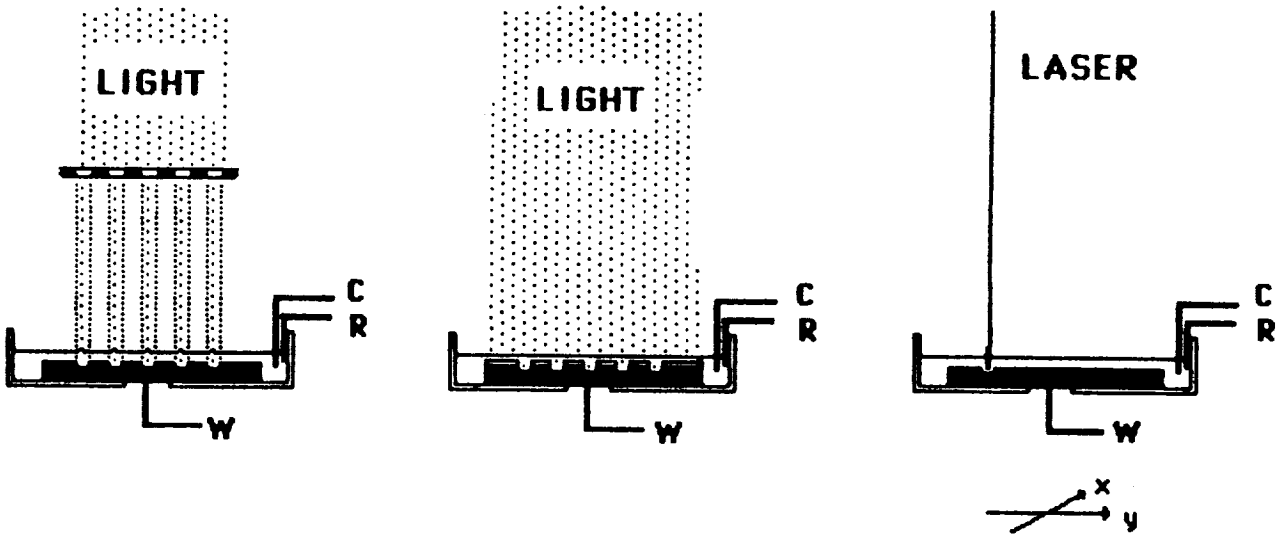

Figure 2. Schematic view of techniques for photoelectrochemical etching of periodic structures. W, C, and R denote working, counter and reference electrodes, respectively.

2.0 PHASE I RESULTS

2.1 Overview

Discussions with NASA/Goddard technical personnel which took place during Phase I provided us with insights into their needs, which were primarily for low pitch Eschelle gratings to be used in spectrographic instruments in a second generation space telescope [7]. As such, having demonstrated the basic feasibility of photoelectrochemical etching using interferometry and laser scanning (Section 2.5), we chose to emphasize those techniques likely to yield a controllable groove profile. A major breakthrough in this regard, established in Phase I, was the demonstration that V-grooves, and other profiles, could be produced in mild electrolytes (e.g., 1M KCl) by photoelectrochemical etching of oriented GaAs crystals using mask-defined patterns (Figure 2b).

These results also led us to emphasize GaAs in our Phase I work, rather than Si and/or ZnSe originally proposed. The choice was based on availability, cost, well-documented physical properties, and well-behaved photoelectrochemical properties. Unlike Si, trivalent Ga and As species, the products of GaAs photodissolution, are highly soluble in a wide variety of mild electrolytes. Silicon, which is also widely available and inexpenssive, must be used in conjunction with aggressive fluoride (e.g., hydrofluoric acid) or alkaline etchants to dissolve away the tetravalent Si oxidation products. GaAs has a crystal lattice similar to Si, but also has a richer crystal chemistry due to the polar nature of the lattice. We learned in Phase I that the polar lattice is responsible for the variety of different groove structures that can be achieved.

2.2 Photoelectrochemical Etching in n-GaAs: Experimental Approach

Photoelectrochemical etching of mask-defined features in single crystal n-GaAs was examined extensively in Phase I. The phenomenon of photoelectrochemical etching of n-GaAs has been recognized for over 20 years, since the pioneering work of Gerischer (8,9), Pleskov (10), and Haisty (11). It is fairly well established that the anodic dissolution of GaAs occurs by a six electron process (3,8). Faktor and Stevenson (12) have demonstrated that the complexant Tiron (1,2-dihydroxybenzene-3,5-disulfonic acid) can be employed in the electrochemical etching of GaAs without passivation due to the accumulation of insoluble reaction products. These authors succeeded in stripping relatively large amounts of GaAs using this process, for the purpose of depth profiling. Our own survey of electrolytes revealed that even KCl or dilute H_2SO_4 could be used to produce deep photoelectrochemically etched features. However, we found that Tiron was also useful in enhancing the dissolution of passivating oxides that tend to form on the crystal surface during post baking of the resist pattern. Hence, Tiron was the supporting electrolyte of choice for Phase I work.

Single crystals of n-GaAs were obtained from MA-COM/Laser Diode, Inc. Doping levels were 3.2×10^{17} and 1.3×10^{18} cm^{-3} for crystals of (100) orientation and 3.3×10^{18} cm^{-3} for (111) crystals. The wafers were chemomechanically polished by the manufacturer, and no additional surface treatment was provided. Ohmic contact was made to a roughened surface using an In/Ga eutectic. The crystal was placed contact side down onto a horizontal copper base plate, to which electrical contact was made. The electrochemical cell consisted of a shallow dish with a hole drilled in the bottom, typically 0.2 cm in diameter. This hole was placed over a selected area of the polished crystal face, and a liquid tight seal was made with an O-ring.

Electrochemical measurements were conducted with an ECO Model 551 potentiostat/galvanostat, a Princeton Applied Research Model 175 Universal Programmer and an ESC digital coulometer. All photoelectrochemical measurements and etching experiments were made in a 3-electrode configuration, with a Pt counter electrode and a saturated calomel (SCE) reference electrode (Figure 3). Electrolyte solutions containing 0.5M Tiron (Aldrich Chemical Co.) were made from triply distilled water and had a pH of 3.4. Light sources used in this work were a Uniphase 1 mw HeNe laser and a Omnichrome 14 mw HeCd laser (operating at 632.8 and 442 nm, respectively), and a broad band 150W Xe lamp. Appropriate optics were used to present a uniform illumination to the exposed electrode surface. Light intensities were adjusted using neutral density filters and were measured with a United Detectors 10DP photodiode. All photoelectrochemical measurements were corrected for reflective losses. Reflectance from the crystal surface was determined in this laboratory using a Cary 14 spectrometer with a near normal specular reflectance attachment. The result was 0.31 at 633 nm and 0.41 at 442 nm, in agreement with published values (13). It was also necessary to make a small correction for the absorbance of the Tiron electrolyte, which was determined for each light source using the photodiode and a known path length of solution.

Patterns were produced on the GaAs surface in Shipley 1350J positive photoresist, spun on and developed according to the manufacturer's instructions. Metallization was achieved using the lift-off technique after thermal evaporation of 200 nm of Cr followed by 500 nm of Au.

2.3 Photoelectrochemistry of n-GaAs in 0.5M Tiron

Current-voltage curves were recorded in the dark and under illumination of n-GaAs at several doping levels and crystal orientations in 0.5M Tiron electrolyte. The dark currents under reverse bias were sensitive to surface preparation. At potentials >1V, "leakage" currents have been observed at levels >1 mA/cm^2 for abraded surfaces. However, as shown in Figure 4, the chemomechanically polished surfaces used in our experiments showed anodic currents that were very much lower. The crystals of (100) orientation with the lower doping level displayed dark anodic currents of <10 $\mu A/cm^2$ to beyond 1V. At doping levels $>10^{18}/cm^3$, dark anodic currents of 10-100 $\mu A/cm^2$ were observed. This type of behavior is consistent with an avalanche breakdown model, described by Tranchart et al. (14). However, of relevance here is that all crystals exhibited a region of dark anodic current <10 $\mu A/cm^2$ out to at least 0.5V positive of the onset of cathodic current. This is the prime region for high photoetching selectivity.

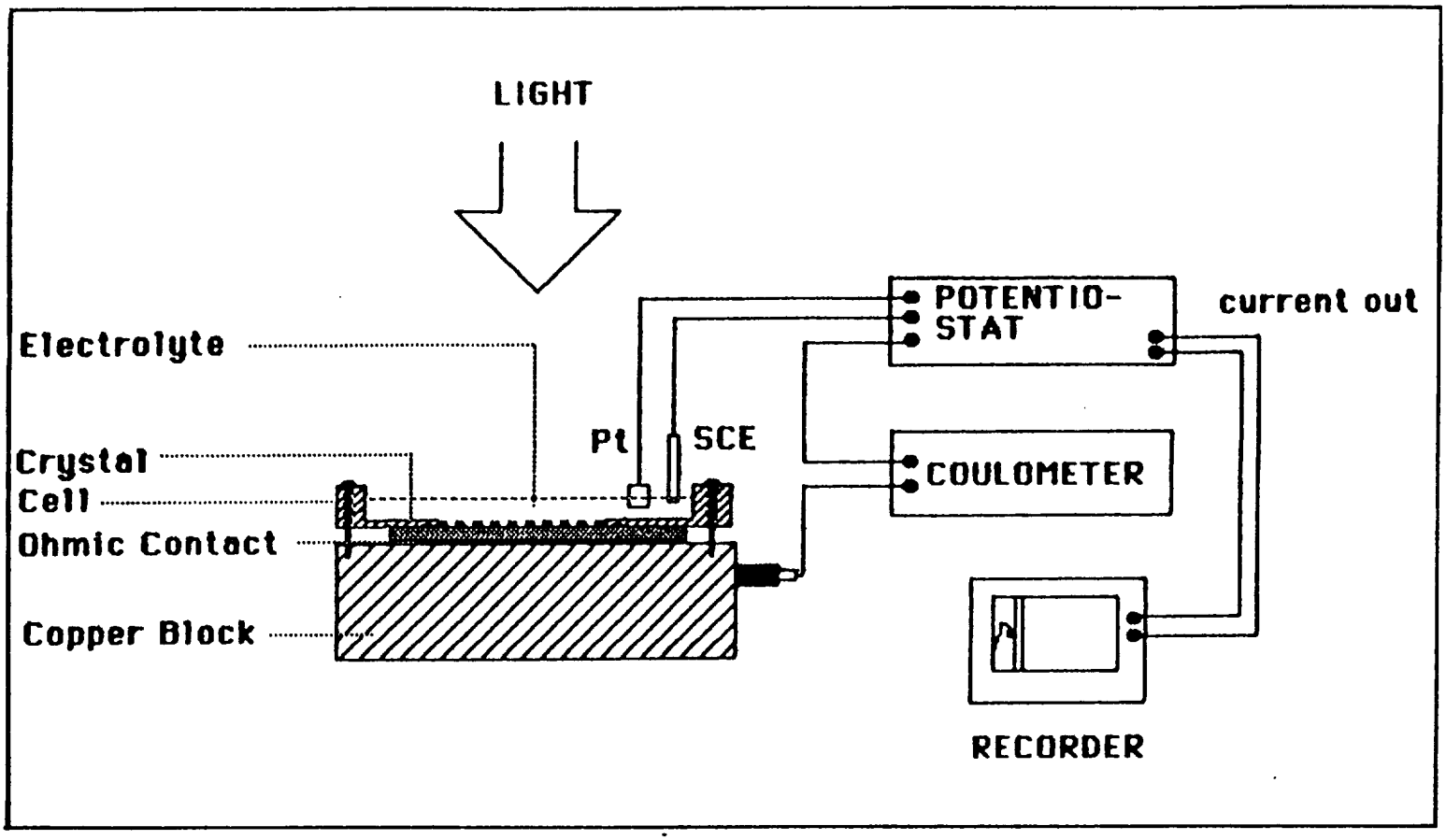

Figure 3. Cell and associated electrochemical instrumentation for controlled photoelectrochemical etching of masked grating structures.

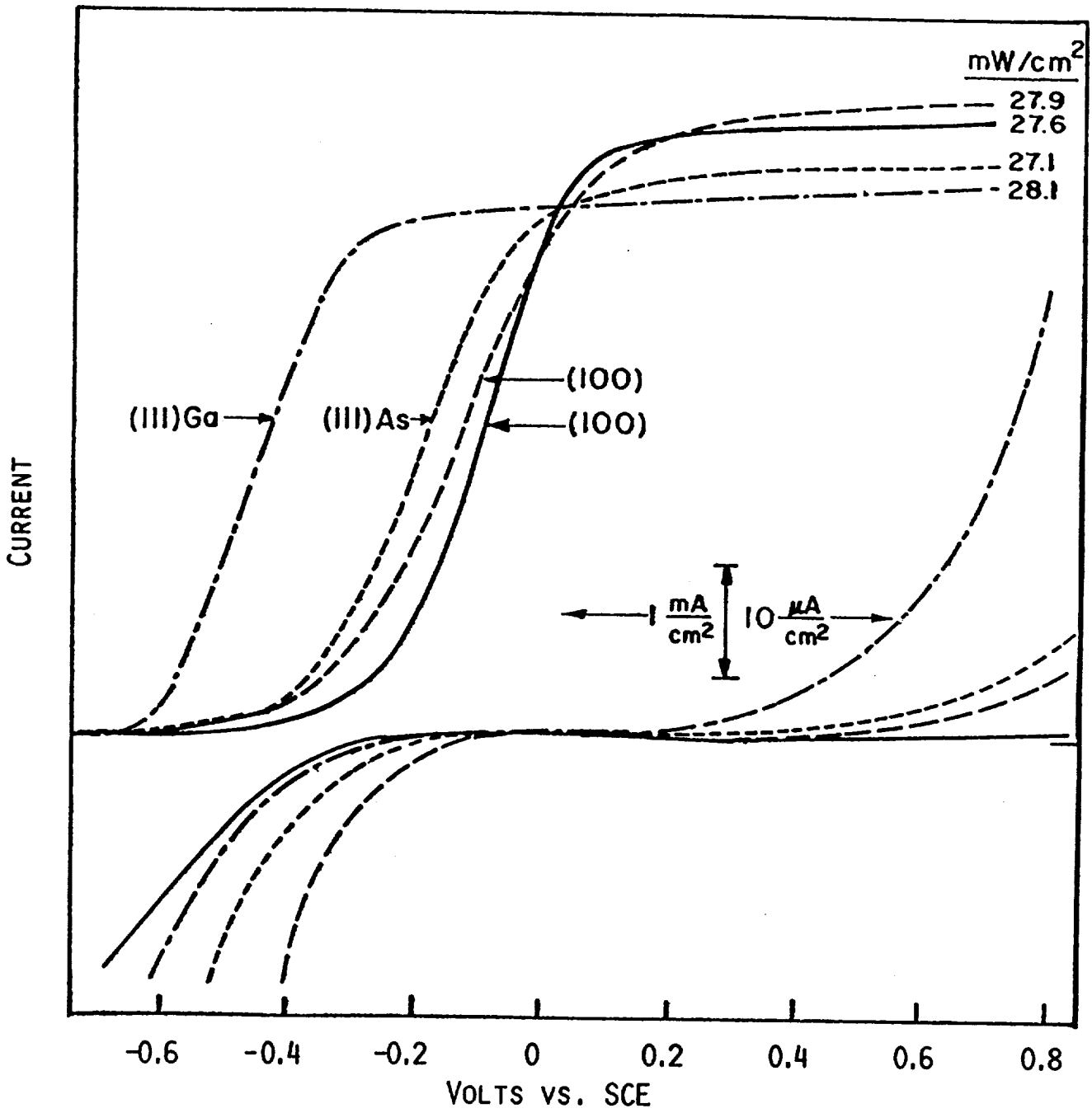

Figure 4. Linear sweep current-voltage curves for n-GaAs in 0.5M Tiron electrolyte, in the dark and under 442 nm illumination. Doping levels: (——) $3.2 \times 10^{18}/cm^3$, (— —) $1.3 \times 10^{17}/cm^3$, (---, — - —) $3.3 \times 10^{18}/cm^3$. Sweep rate, 200 mV/sec, Light intensities are shown in the upper right.

Photocurrent-voltage curves for the (100), (111)Ga and (111)As orientations are compared in Figure 4 using 442 nm excitation. All n-GaAs crystals displayed high photosensitivity and photon limited currents under positive bias. The onset of photocurrent was -0.5 to -0.6V, in agreement with Faktor and Stevenson (12). The onset is approximately 500 mV positive of the reported flat band potential at pH 3.4 (15), indicating considerable kinetic inhibition and carrier recombination at the semiconductor/electrolyte interface (16). The (111)Ga face exhibited a steeper rise in the photocurrent onset than the other orientations, reaching photon limitation at approximately -0.1V. Photon limited currents were obtained at >0.1V for the other crystals. Kohl and co-workers observed a similar effect for the photoelectrochemical etching of n-GaAs in mineral acids (3).

The photon limited currents were measured for each crystal at 442 nm and 633 nm over intensities ranging from approximately 10 $\mu W/cm^2$ to 10 mW/cm^2. In each case, a linear relationship was observed. The following relationship can be derived from the current equivalent of the photon flux:

$$i(A/cm^2) = 8.065 \times 10^{-4} \lambda I \phi (1-R) \qquad [1]$$

where λ is the wavelength in nm, I is the intensity in W/cm^2, ϕ is the quantum yield and R is the crystal reflectance. At 442 nm and 633 nm, the slopes of i vs. I plots are equal to 0.21ϕ and 0.33ϕ, respectively, using the values of R cited earlier. Table 1 summarizes the quantum yields obtained from the least squares fits of these slopes. The quantum yields were highest for shorter wavelengths and lower doping densities, in agreement with a simplified Gartner "Schottky barrier" model of electrode behavior under reverse bias (17,18). Also included in Table 1 are the calculated values of αW, where α is the optical absorption coefficient (in cm^{-1}) and W the space charge width at 0.2V polarization. W is a measure of the depth to which the bands are bent beneath the semiconductor surface, as illustrated in Figure 1. Electrons and holes created beyond this region are likely to be inefficiently separated. In most cases of crystals used in these studies, αW is less than unity indicating that the loss mechanism for photogenerated holes at this applied potential is probably bulk recombination.

2.4 Photoelectrochemically Etched Profiles

A Ronchi ruling mask having 100 cycles/mm was used to pattern the (100) crystals along the [01$\bar{1}$], [010] and [011] directions, as illustrated in Figure 5. The patterns were produced as Cr/Au, or as photoresist alone. Photoelectrochemical etching was performed with a Xe white light source. Etching reactions were carried out at a fixed potential in the photon limited region, typically 0.2V. However, no differences were found in the range 0.2 to 0.8V, so the potential was usually set about 200 mV positive of the onset of photon limitation. For most experiments, the intensity of the Xe source was set at 300-400 mW/cm^2, sufficient to give a dissolution current of about 10 mA/cm^2 of geometric area, or since the grid lines occlude 50% of the surface, 20 mA/cm^2 of exposed GaAs. Some additional dark anodic current was seen to arise from the Cr/Au grid contacts, but this still amounted to <1% of the photocurrent. The profiles of the grooves etched along the different directions were observed on cleaved samples using scanning electron microscopy.

Table 1

Experimentally observed limiting quantum yields at 442 nm and 633 nm for photocurrent generation in n-GaAs in 0.5M Tiron electrolyte. V = 0.2V vs. SCE. Results corrected for reflectance and absorption by the electrolyte.

Orientation	$N_d(cm^{-3})$	λ(nm)	αW [a]	ϕ [b]
(100)	3.2×10^{17}	442	1.2	0.92
		633	0.3	0.70
	1.3×10^{18}	442	0.6	0.92
		633	0.1	0.62
(111)Ga	3.3×10^{18}	442	0.4	0.84
		633	0.1	0.60
(111)As		442	0.4	0.88
		633	0.1	0.61

[a] Values of W taken from W. S. Hobsen and A. B. Ellis (J. Appl. Phys., 54, 5956 (1983)), for similarly doped crystals under equivalent conditions of reverse bias. These experimental values are close to those calculated using the depletion approximation. Absorption coefficients used were $\alpha_{442} = 2 \times 10^5$ cm^{-1} and $\alpha_{633} = 4.4 \times 10^4$ (13).

[b] Determined for intensity range of 0.02 to 2 mW/cm^2.

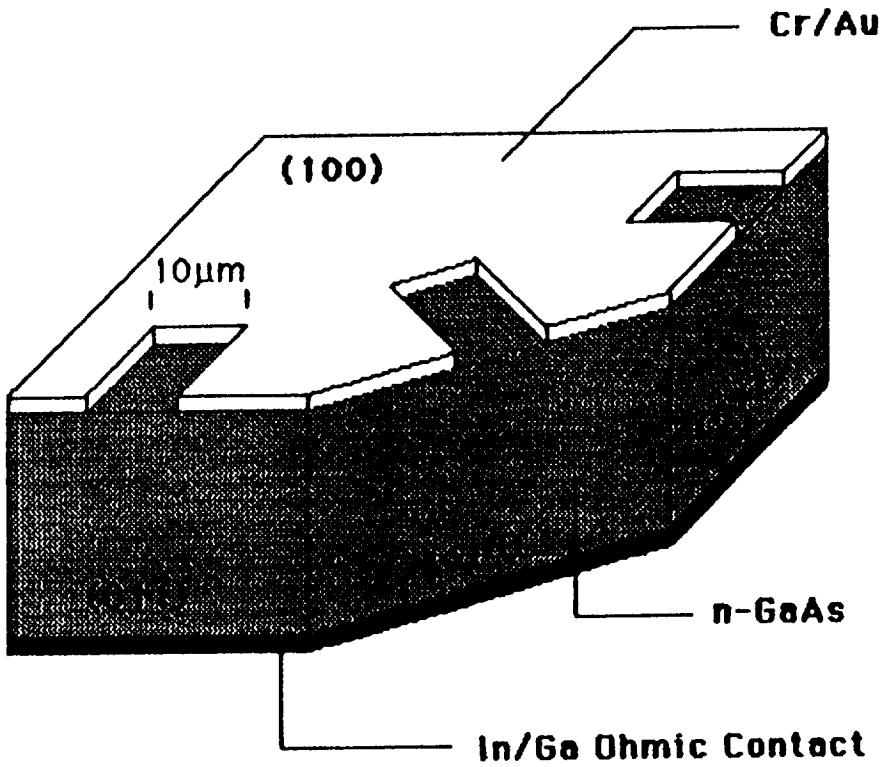

Figure 5. Patterning of (100) n-GaAs crystal surface for groove etching experiments.

Figure 6 shows the profiles of grooves that formed after removal of 11 C/cm^2 of exposed (100)GaAs surface for crystals of the two different doping densities. The profiles are obviously not solely defined by the photon flux. The lower doped crystals develop V-shaped grooves along the [011] direction, which form as a result of undercutting the mask. The grooves have a crystallographic angle of approximately 54°, and are thus a result of exposure of the (111)Ga plane. The same kind of profile is observed with some oxidizing chemical etchants in the dark, such as H_2SO_4-H_2O_2-H_2O (19) and Br_2/methanol (20,21). The other two orientations give rise to more rounded profiles, indicative of a relatively isotropic process, also with analogies in chemical etching. It is evident that considerable etching takes place beneath the shadowed region of the mask, which remained largely intact. In contrast, cross sections of etched grooves in the more highly doped (100) crystals showed relatively little undercutting. The [011] grooves display a pointed bottom, again indicative of the retarded reaction along the (111)Ga plane. Thus, the doping level is a key variable in photoelectrochemical etching of high aspect ratio structures.

Grooves were next etched to the extent of 120-160 C/cm^2 along the [01$\bar{1}$] and [010] directions of the more highly doped (100) crystals. Cross sections of the resulting structures are shown in Figure 7. It can be seen that the basic features shown in Figure 6 are carried through in these deeper grooves. The vertical walls of the [01$\bar{1}$] grooves are noticeably thinned by the tendency to reveal the (111)Ga plane during the etching, possibly enhanced by oblique reflections off the angled bottom. This thinning is constant throughout the depth of the structure. The other orientations exhibit grooves with some undercutting near the grid, but which narrow to a constant width as the etching proceeds (only the [010] groove structure is shown).

A charge of 2.12 C/cm^2 is required to etch 1 μm of GaAs, assuming a 6e$^-$/mole stoichiometry. At the average current of about 20 mA/cm^2 used here, the etch rate of the grooves is approximately 0.01 μm/sec assuming no undercutting. The coulombs required to etch the structures in Figure 7 are indicated in the captions. In each case, the depth is less than theoretically possible because of the undercutting phenomenon. Similarly, the time required for etching to a given depth is greater than theoretically predicted from the photocurrent.

It is interesting to note that the type of masking material can be used to control groove shape. Experiments with photoresist masks show that they are more readily undercut than Cr/Au, and that they tend to float off in segments during the undercutting process instead of remaining intact like the Cr/Au. For example, the result of etching the groove in the [01$\bar{1}$] direction using the lower-doped n-GaAs and a photoresist mask of the same dimension as the Cr/Au mask was also a sawtooth profile, depicted in various stages of development in Figure 8. The photocurrent increases gradually during the etching process, as shown in Figure 9, due to the undercutting of the resist stripes by the growing sawtooth. A maximum is finally reached when the grating is complete. Note that the depth of the etched features can be controlled by monitoring the total coulombs passed, while the rate of etching is precisely controlled by the light intensity. Symmetrical grooves

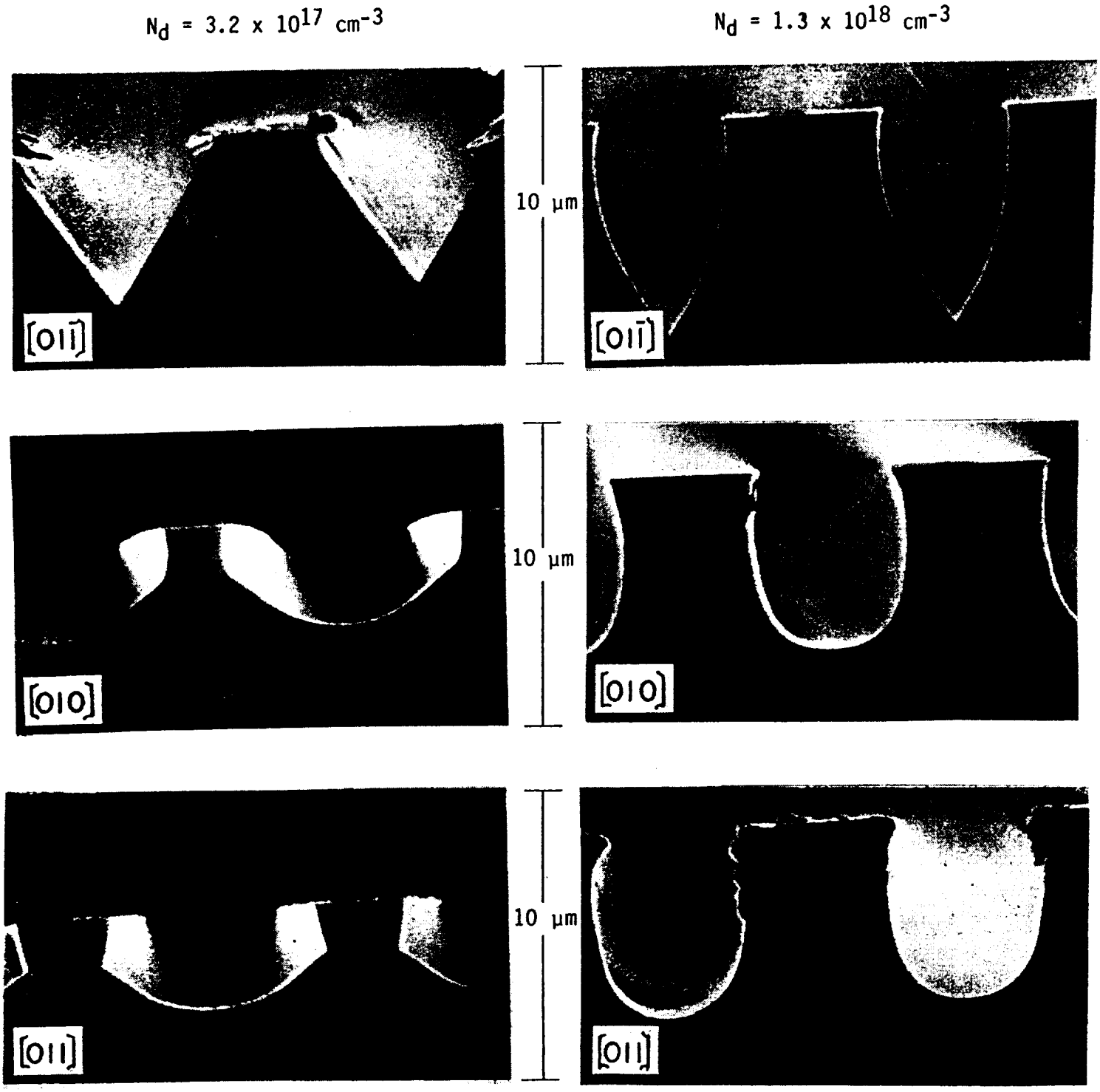

Figure 6. Scanning electron micrographs of cross sections of photoelectrochemically etched grooves in (100)n-GaAs, showing effects of groove orientation and doping level. Electrolyte is 0.5M Tiron; light source is 150W Xe, intensity adjusted to give photocurrent of ~20 mA/cm^2. Potential = 0.2V vs. SCE; charge = 11 C/cm^2.

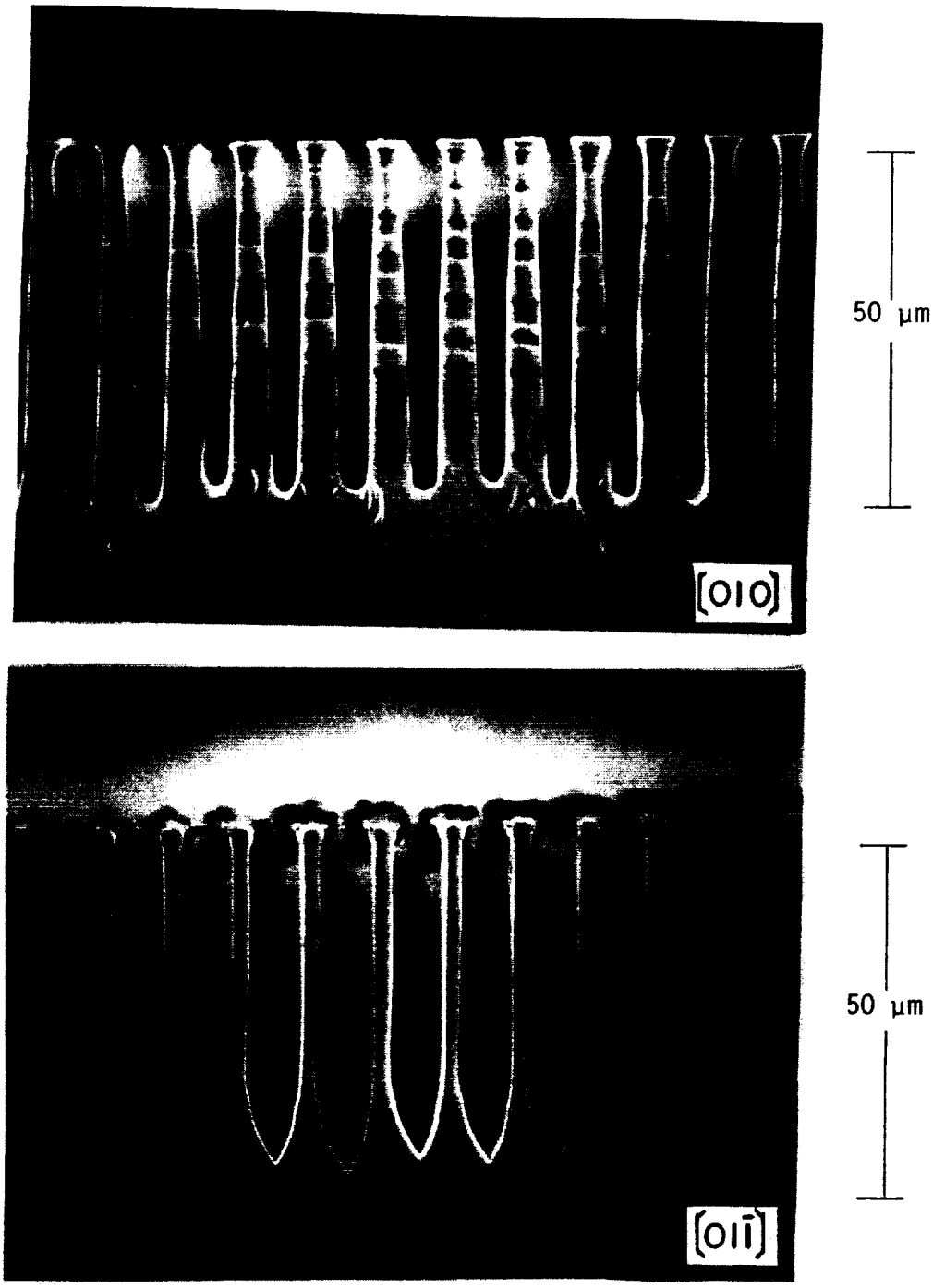

Figure 7. Scanning electron micrographs of cross sections of photoelectrochemically etched grooves in (100)n-GaAs: Top 121 C/cm^2, bottom 157 C/cm^2. Same conditions as Fig. 6.

Figure 8. Scanning electron micrographs showing cross sections of grooves photoelectrochemically etched in (100)n-GaAs, [01$\bar{1}$] direction, at three stages of development.

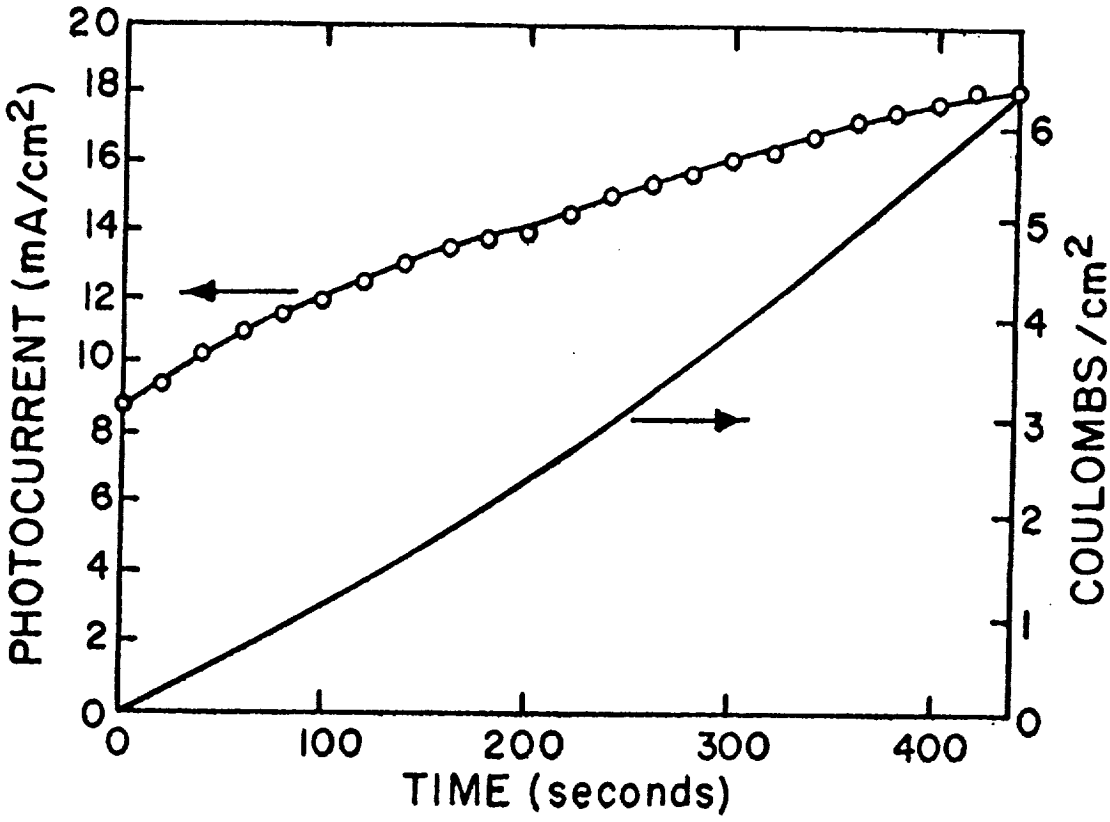

Figure 9. Time evolution of photocurrent and charge for etching V-grooves in n-GaAs, shown in Figure 8.

spaced 10 μm apart will have a depth of 7.14 μm. The theoretical volume of GaAs removed to form these grooves over 1 cm^2 is 3.57 x 10^{-4} cm^3 or 8.07 coulombs/cm^2 assuming 6 equivalents/mole (3). Typically, we observed that 10-20% less total charge is required. This may be due to a lower stoichiometry for the dissolution reaction in the Tiron electrolyte.

In the fabrication of sawtooth structures in lower doped n-GaAs using the metal mask, the tenacity of the mask increases the dimension of the shadowed region as etching proceeds, resulting in greater downward etching than with photoresist. As a consequence, fully formed grooves etched with the metal mask have a profile steeper than 54°. An example of such a grating is shown in Figure 10, which represents the structure in Figure 6 (top left) after photoelectrochemical etching to the extent of 22 c/cm^2. This amount of charge permits the grooves to fully form, the Cr/Au mask floating off when the two sides meet to produce the pointed apex. Grating structures made under the same conditions, but utilizing a photoresist mask, retain the crystallographically imposed 54° blaze angle (22).

A few preliminary experiments were conducted to show the effect of oblique illumination of the patterned electrode surface. The result of illumination at 30° in the high doped crystal is shown in Figure 11. The far wall is the crystallographically defined (111)Ga surface, but the blazed wall is nearly representative of the light flux since the near (111)Ga surface is shaded. The somewhat concave nature of the blazed surface may be due to the same solid state, diffusional process giving rise to rounded profiles in Figure 6. This experiment nevertheless demonstrates the feasibility of achieving blazed grooves using oblique illumination, and represents one approach to be examined further in proposed Phase II work.

The degree to which photoelectrochemical etching of the patterned (100)n-GaAs surface follows the masking pattern is doubtless dependent on many factors, such as diffraction (23) and wavelength of the light source. However, in the series of experiments conducted in Phase I, the only material variable was the doping density, N_d. The resolution of holographic diffraction gratings photoelectrochemically etched in the surface of n-InP has been considered in detail by Ostermayer and co-workers (24). They too found that resolution increased with increased doping. The doping density will affect several semiconductor transport properties, including W (Table 1) and the diffusion length of charge carriers ($l_{n,p}$), both proportional to $N_d^{-1/2}$. Impurity scattering associated with increased doping also decreases the carrier mobilities (μ) (13), and hence their diffusion coefficients according the the Einstein relationship $D = \mu(kT/q)$. The results of Ostermayer et al. (24) indicate that a high reaction velocity at the interface is key to achieving good resolution. Essentially, when the reaction velocity is low, the photogenerated holes can spend much more time accumulated at the interface than they do in getting from the point of generation to the interface. Hence, it is this interfacial region where most of the lateral diffusion associated with the loss of resolution occurs. It is argued by these workers that the narrower depletion region associated with higher doping causes holes to accumulate closer to the surface, and hence not to diffuse as far laterally before they are consumed by reaction. The lower implied value of D_p for more highly doped crystals also acts to increase resolution by reducing lateral diffusion.

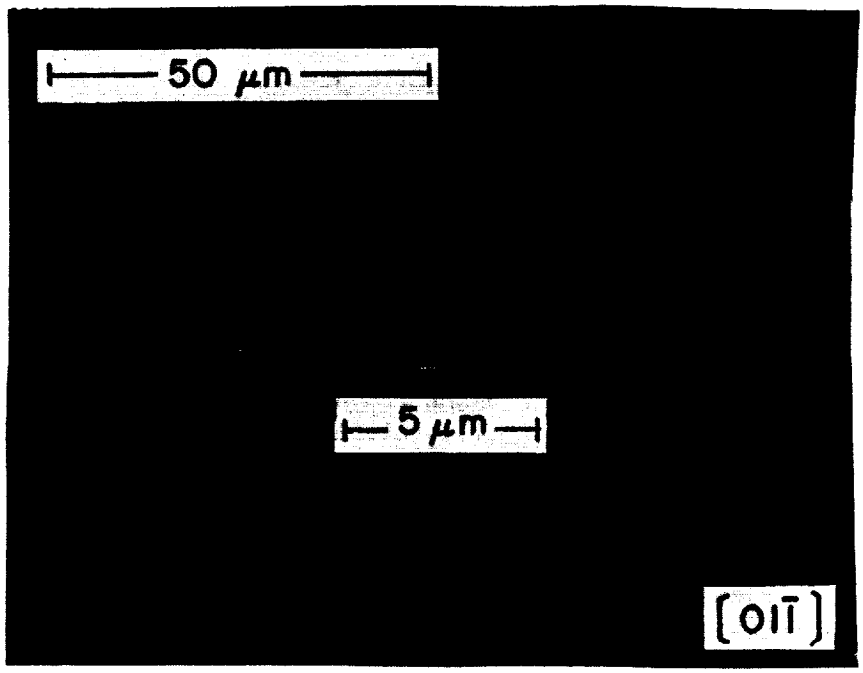

Figure 10. Sawtooth profile of grooves photoelectrochemically etched in (100)n-GaAs, [01$\bar{1}$] direction; N_d = 1.3 x $10^{17}/cm^3$; charge = 22 C/cm^2; Cr/Au mask.

Figure 11. Blazed groove in (100)n-GaAs formed by photoelectrochemical etching of [01$\bar{1}$] oriented slot at 30° incidence. (150W Xe source, N_d = 1.3 x $10^{18}/cm^3$, V_{bias} = 0.2V, 0.5M Tiron electrolyte, Au/Cr mask).

If neither minority carrier diffusion nor differential crystallographic reactivity were significant, photoelectrochemical etching strictly modulated by the photon flux would be expected. This behavior is most closely approached for the higher doped crystals, particularly for grooves oriented away from the [01$\bar{1}$] direction. Because of its dependence on N_d, the primary source of undercutting must be lateral diffusion of holes, at least initially. Further undercutting might be expected due to light trapping beneath the growing lip of the mask. This could explain the tendency toward more significant etching in the region just beneath the mask, compared to deeper within the groove.

Rounded groove profiles are indicative of etching isotropy controlled by diffusion. Round-bottomed structures are observed in all but the [01$\bar{1}$] direction, where kinetic effects due to crystallographic orientation contribute. Their shape represents the steady-state population of interfacial holes, distributed statistically according to the diffusional process.

Both chemical oxidants and light operate by the initial injection of positive charge carriers (holes) into the semiconductor (25). The etching chemistry of the (111) planes of GaAs has shown that the Ga and As polar surfaces have vastly different reactivities toward chemical oxidants (26). Triply bonded (111)As surface sites are expected to have associated lone pair electrons which form a band within the forbidden gap; triply bonded Ga on the (111)Ga surface has "empty" dangling bonds (27). The As sites apparently foster hole trapping and, at low bias, surface recombination. This may explain the steeper rise of the photocurrent-voltage curve for the (111)Ga crystals in Figure 4. At potentials corresponding to photon limited photocurrents, hole trapping on nucleophilic interfacial As is the initiating step in dissolution which, if orientationally possible, will be consumed in a laminar fashion (28). This will be followed by the rapid removal of the highly labile underlying "single bonded" Ga atoms. Holes will have a low affinity for (111)Ga compared to (111)As or even other faces with mixed composition. Basically, once the holes are injected, their equilibration and reaction at the surface will be according to the differential reactivity of interfacial sites. In this way, the mechanism for exposure of the (111)Ga plane is similar for both chemical and photoelectrochemical etchants.

2.5 Direct Writing of Gratings Using Laser Scanning

An alternative approach for photoelectrochemical etching of gratings was investigated during Phase I, involving laser scanning techniques. The apparatus for conducting these experiments is shown in Figure 12. The laser beam is spatially filtered, collimated, and finally focused to a spot on the crystal electrode surface. The cell was similar to that shown in Figure 3. However, most experiments were carried out without an electrochemical assist, i.e., with the crystal simply immersed in a mildly etching electrolyte. In this case, 10% KOH was employed throughout. With this arrangement, light directed onto the crystal surface increases the concentration of holes in the illuminated region. This sets up a localized corrosion reaction, mediated by the electrolyte. The crystal oxidizes where light is absorbed, and a complementary solution reaction occurs in neighboring dark regions. In the case of n-GaAs, the overall corrosion reaction is

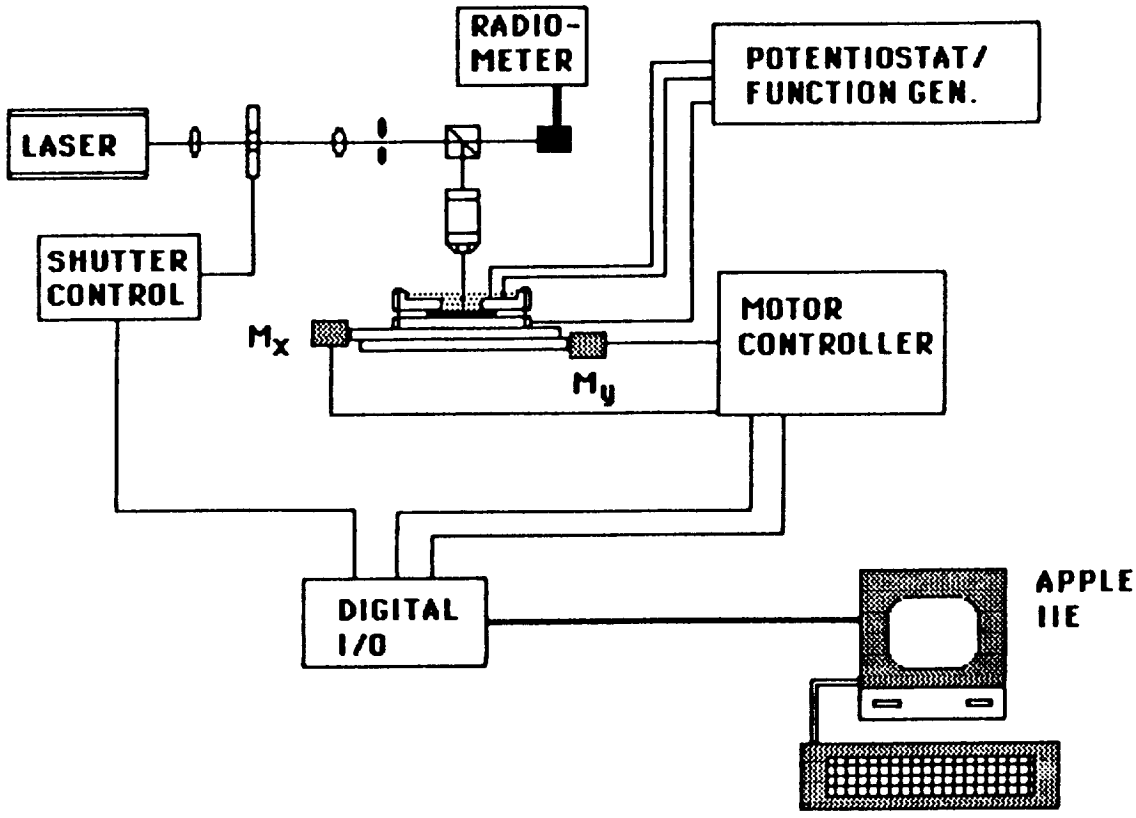

Figure 12. Programmable laser etching apparatus. M_x and M_y are stepper motors. The focusing optic is typically a 10X microscope objective.

$$GaAs \rightleftarrows Ga(III) + As(III) + 6e^- \quad (light) \qquad [2]$$

$$6H_2O + 6e^- \rightleftarrows 3H_2 + 6OH^- \quad (dark) \qquad [3]$$

This is often referred to as "photochemical" (PC) etching, as opposed to photoelectrochemical (PEC) etching. The difference is illustrated in Figure 13. Since the electrode is not anodically biased into the photon limiting region in the PC process and since there are high overpotentials associated with the "dark" reaction, the quantum yields for the PC process tend to be <1% of the PEC process.

Gratings were drawn in the crystal surface by raster scanning the cell using X and Y stepper motors (Oriel). These were capable of 1.25cm travel in 1 μm steps at 500 steps/sec. The line spacing length and direction of travel were all directed by an Apple IIe computer, which operates using TTL pulses to the motor controllers (29).

The sensitivity of the n-GaAs/10% KOH interface to etching under focused laser illumination has been discussed by us earlier (30). The result of that work is summarized in Figure 14. When a single hole is etched using the tightly focused laser (spot size 2-5 μm), the observed diameter of the hole at the crystal surface is a function of total exposure energy (intensity x time). The holes tend to broaden at high energies, a probable result of the lateral spreading of holes described earlier in this report. What this means is that we are confined to shallow structures with this technique, at least with visible light and intensities high enough to permit a reasonable rastering rate. As shown in Figure 14, holes of <5 μm diameter could be formed at up to ~500 Joules/cm^2 exposure.

When the cell is translated, there is a certain amount of leveling of the substrate which is required. The He-Ne laser gives a gaussian beam profile, with a focused beam waist of radius, W_o, typically ~1μ here. The ±5% depth of focus is given by

$$\Delta_z = \frac{0.32\pi W_o^2}{\lambda} \qquad [4]$$

For our optical arrangement, Δ_z = 2μ, so extreme flatness is required.

Shallow gratings were produced by scanning at a rate of 350 steps/sec using a beam with a 10^4 W/cm^2 focused intensity. The resulting dwell time at each "step", separated by 1μ, was 0.003 sec, giving an energy of 30 J/cm^2 per point. The best gratings were produced by multiple passes at this intensity, in which a total energy of 60 to 300 Joules/cm^2 per point was accumulated. This produced a more linear groove than if the scan rate were reduced, which resulted in a more scalloped appearance. Examples of gratings etched using 3 and 5 passes are shown in Figure 15.

A profilimeter profile of the structure in Figure 15 is shown in Figure 16. The profile shows grooves <0.2μ deep, and with a depth variation indicative ofthe considerable roughness revealed in Figure 15. This roughness probably originates from the very high etching rates involved here, approximately 50 μ/sec!

"PHOTOCHEMICAL" ETCHING

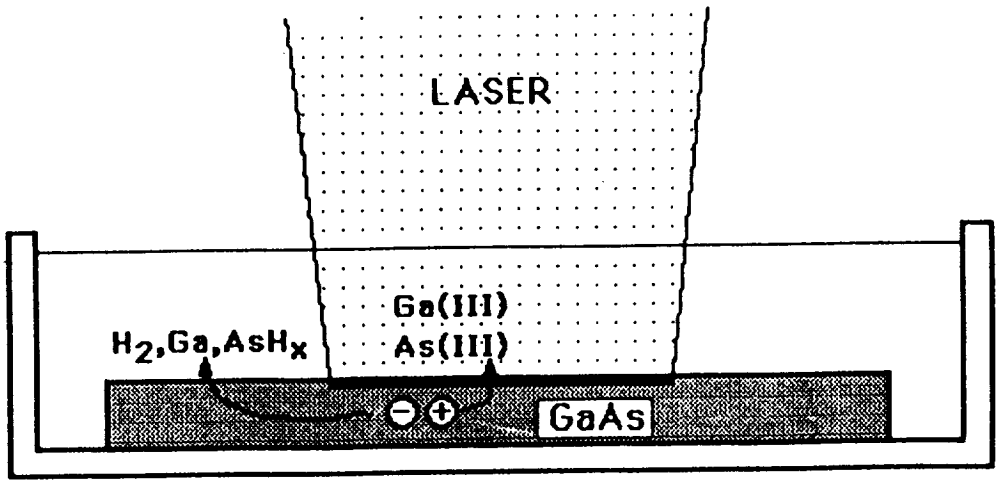

PHOTOELECTROCHEMICAL ETCHING

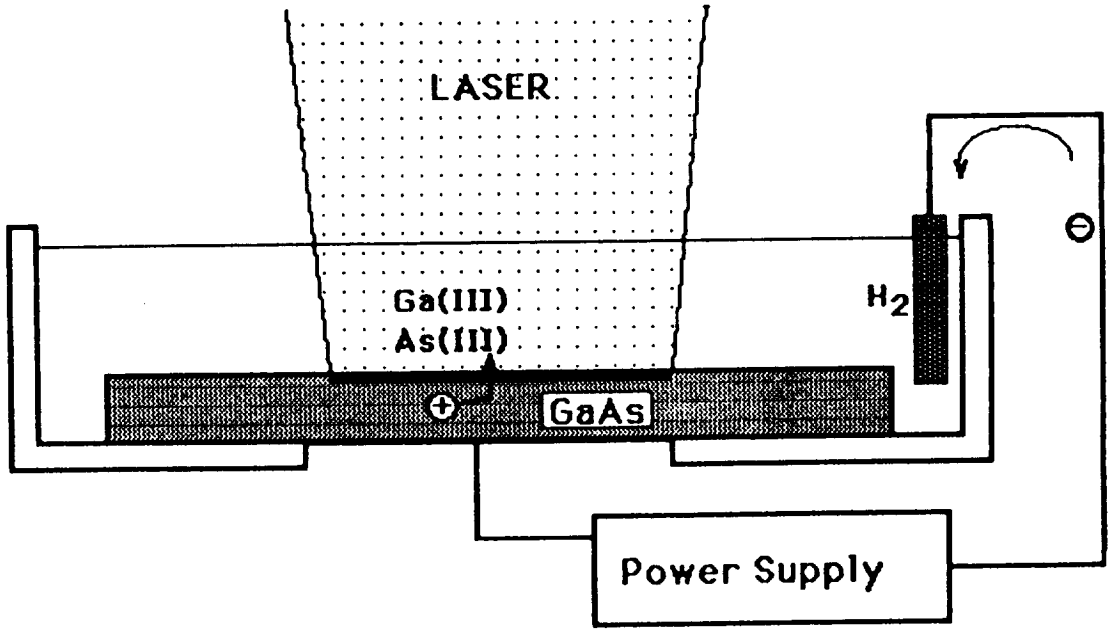

Figure 13. Photochemical and photoelectrochemical etching arrangements.

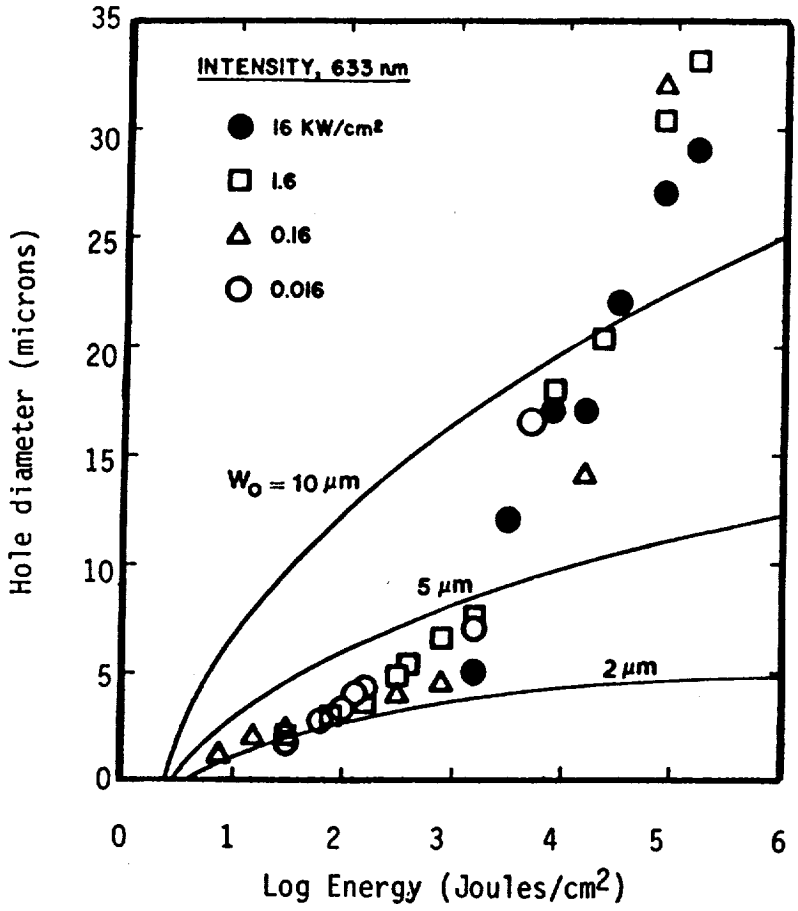

Figure 14. Etched hole diameters vs. exposure energy for 2 μm diameter laser spot on n^+-GaAs in 10% KOH; also, theoretical diameters at >0.1 μm depth for a gaussian beam profile (from ref. 30).

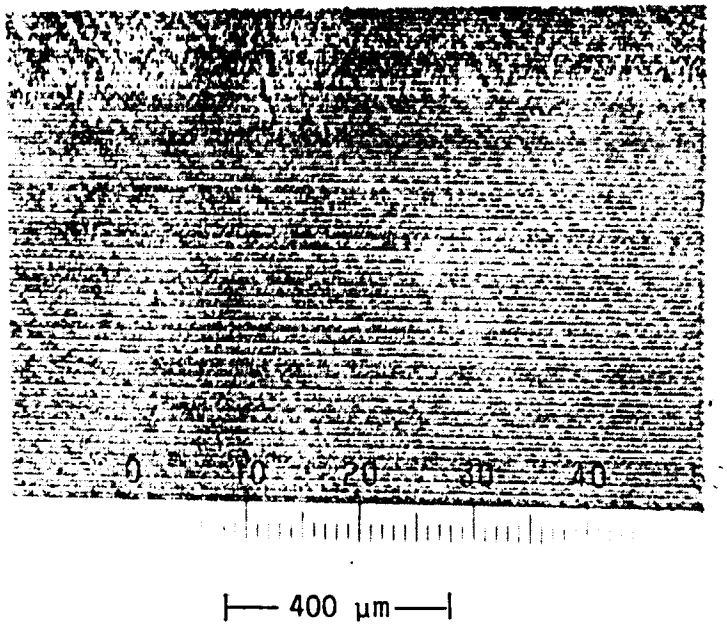

Figure 15. Photoetching of gratings in (111)n-GaAs/10% KOH with a scanned HeNe laser.

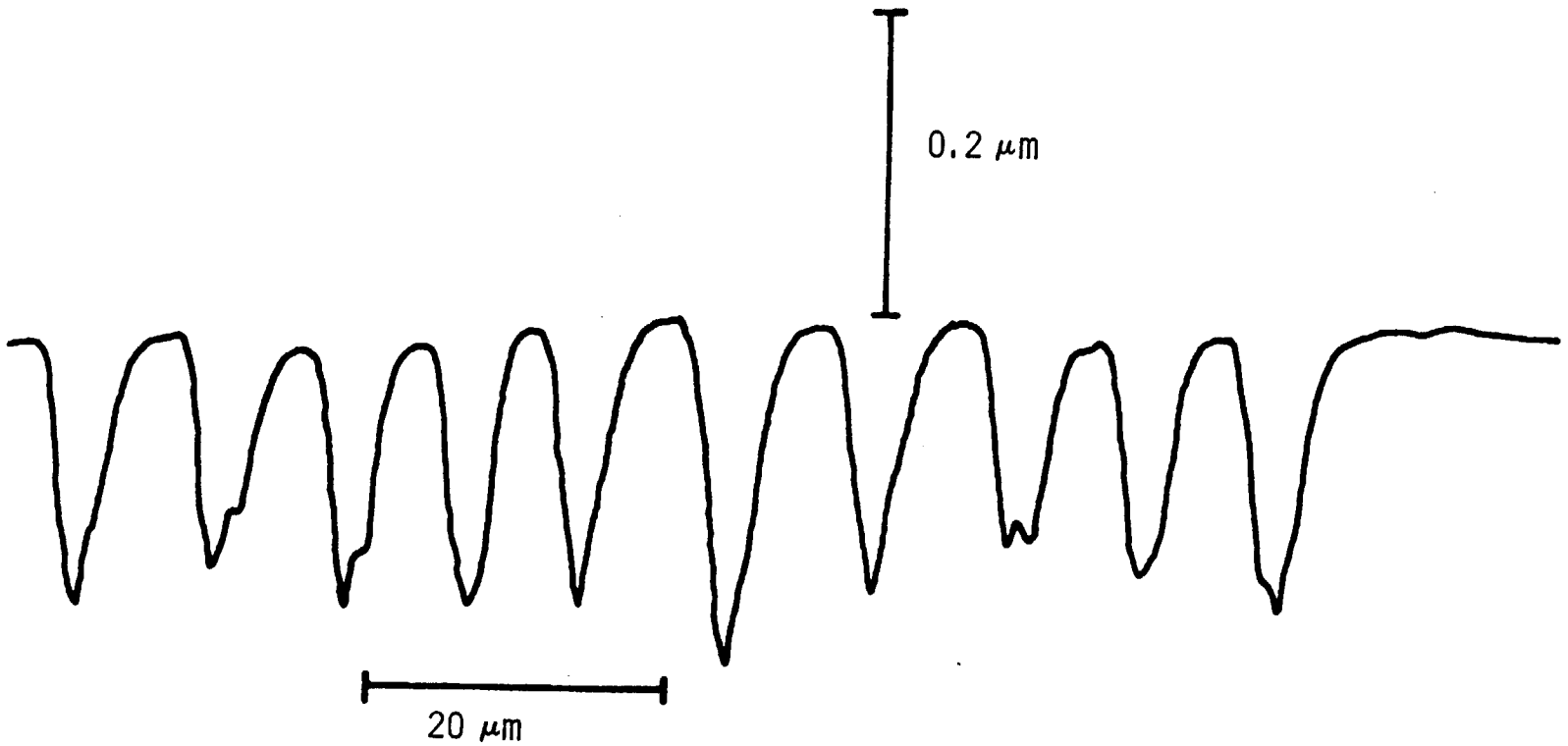

Figure 16. Dektak profile of grating etched with scanned focused 633 nm laser in (111)n-GaAs.

Figure 17 shows the first order diffraction from a surface grating built up with 1 pass and 3 passes of the laser. The intensities of the diffracted lines were measured with an EG&G model 451 radiometer. It is seen that only after 3 passes is sufficient groove depth built up to show a significant diffraction effect. The roughness of the features gave rise to rather severe light scattering between the diffracted orders. The gratings shown in Figure 15 are therefore obviously not suitable for spectroscopic applications. These studies did show, however, the feasibility of direct ruling of periodic structures using laser light. The main problem is an uncontrollable roughness and groove profile. The latter is particularly restricted by the gaussian beam shape. Recent results by Podlenik and co-workers (31) using deep UV focused lasers at an intensity equal to 0.1 to 1% of that which we employed have shown that deep holes and grooves can be drilled in GaAs photoelectrodes. The rate of drilling under these conditions, ~0.2 μ/sec, makes the direct laser ruling of large area gratings a very time consuming process. Possibly, a photoelectrochemical (PEC) approach combined with UV laser illumination will yield grooves of sufficient quality at a sufficient rate for practical fabrication of some kinds of laminar spectroscopic gratings.

Passes	Total Energy (J/cm^2)	$\frac{I_0}{I_{00}}$	$\frac{I_{+1}}{I_{00}}$	$\frac{I_{-1}}{I_{00}}$
1	30	.85	.07	.07
3	90	.46	.25	.13

$n\lambda = d(\sin\alpha + \sin\beta)$

I_{00} = Intensity reflected from polished surface

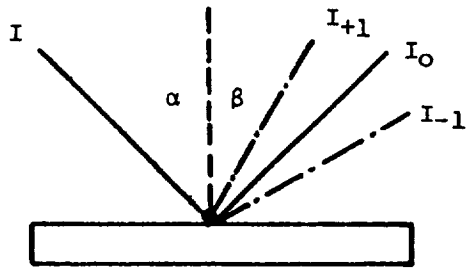

Figure 17. Relative efficiencies of gratings in n-GaAs drawn by 1 and 3 passes of a focused He-Ne laser (see text).

3.0 CONCLUSION

The general conclusion from Phase I is that crystallographically enchanced photoelectrochemical etching is a promising method for fabrication of Eschelle gratings, while direct laser drawing of gratings is probably unsatisfactory for the present application. With regard to the former process, we succeeded, in Phase I, in fabricating small area (<1 cm^2), symmetrical V-groove grating structures with a blaze angle of 54°. A sample was submitted to NASA/Goddard for evaluation. The gratings appear to have a smooth surface morphology as shown in Figure 18. The fact that the etching rate can be controlled means that diffusional gradients in the liquid, which would impair the uniformity, can be minimized. Thus, it is likely that the approach can be used to make large area gratings using illuminators designed for homogeneous exposure. It is also important to note that the very mild electrolytes used in photoelectrochemical etching of GaAs are compatible with virtually all resist or mask materials.

There are several additional areas for improvement that will doubtless extend beyond the scope of the present program and will require working with NASA technical staff. For example, the gratings will require a high degree of linear accuracy of the grooves - up to 1 in 10^5 in the most severe cases - which is beyond the capabilities of conventional mask technology. Although this project cannot address that problem directly, we will be able to use masks which may be developed at NASA or elsewhere to enhance our process. Another example is the quality and size of crystals available for this work, which may be limiting in the most demanding applications.

Although the grating shown in Figure 18 demonstrates the technical feasibility of the photoelectrochemical fabrication of Eschelles, further work is necessary on the photoelectrochemical process itself to generate truly practical structures. A considerable portion of Phase II research, for example, is aimed at modifying the basic photoelectrochemical etching technique to produce V-grooves at alternative blaze angles. Factors which determine the microroughness of the grooves must be optimized in order to produce useful, large area gratings with minimal stray light scattering.

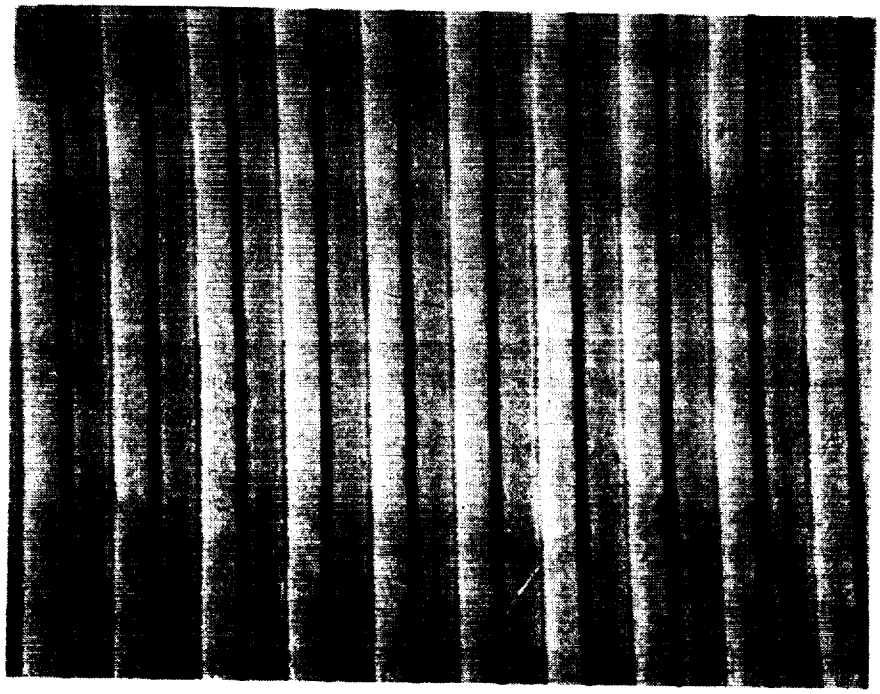

Figure 18. Grating formed by photoelectrochemical etching of grooves in (100)n-GaAs along the [01$\bar{1}$] direction. The grooves were defined in photoresist using a 100 cycle/mm Ronchi ruling mask (V_{bias} = 0.7V, Q = 6.3 C/cm^2, N_d = 3.2 x 10^{17} cm^{-3}).

REFERENCES

1. M. C. Hutley, Diffraction Gratings, (New York: Academic Press, 1982).

2. Y. Y. Gurevich, and Y. V. Pleskov, "Photoelectrochemistry of Semiconductors," Semiconductors and Semimetals, 19, 255 (1983).

3. P. A. Kohl, C. Wolowodiuk, and F. Ostermeyer, Jr., J. Electrochem. Soc., 130, 2288 (1983).

4. Zh. I. Alferov, D. N. Goryachev, S. A. Gurevich, M. N. Mizerov, et al., Sov. Phys. Tech. Phys. 21, 857 (1976).

5. H. Gerischer, J. Electroanal. Chem. 82, 133 (1977).

6. R. Lum, A. Glass, F. Ostermayer, Jr., P. Kohl, A. Ballman and R. Logan, J. Appl. Phys., 57, 39 (1985).

7. B. Woodgate, "Space Telescope Imaging Spectrograph: Executive Summary," NASA Publication STIS-680-85-001, May 1985.

8. H. Gerischer, Ber. Bunsenges. Physik. Chem., 69, 578 (1965).

9. H. Gerischer and I. Mattes, Zeit. Phys. Chem., 49, 112 (1966).

10. Y. V. Pleskov, Doklady Akad. Nauk. S.S.S.R., 143, 1399 (1962).

11. R. W. Haisty, J. Electrochem. Soc., 108, 790 (1961).

12. M. M. Faktor and J. L. Stevenson, J. Electrochem. Soc., 125, 621 (1978).

13. J. S. Blakemore, J. Appl. Phys., 53, R123 (1982).

14. J. C. Tranchart, L. Hollan and R. Memming, J. Electrochem. Soc., 125, 1185 (1978).

15. K. Rajeshwar and T. Mraz, J. Phys. Chem., 87, 742 (1983).

16. J. Reichman, Appl. Phys. Lett., 36, 574 (1980).

17. W. W. Gartner, Phys. Rev., 116, 84 (1959).

18. M. A. Butler, J. Appl. Phys., 48, 1914 (1977).

19. W. Tsang and S. Wang, Appl. Phys. Lett., 28, 44 (1976).

20. Y. Tarui, Y. Komiya and Y. Harada, J. Electrochem. Soc., 118 118 (1971).

18. M. A. Butler, J. Appl. Phys., 48, 1914 (1977).

19. W. Tsang and S. Wang, Appl. Phys. Lett., 28, 44 (1976).

20. Y. Tarui, Y. Komiya and Y. Harada, J. Electrochem. Soc., 118 118 (1971).

21. L. Comerford and P. Zory, Appl. Phys. Lett., 25, 208 (1974).

22. M. M. Carrabba, N. M. Nguyen and R. D. Rauh, submitted to Applied Optics (1986).

23. J. Cheng and P. A. Kohl, Mat. Res. Symp. Proc., 29, 127 (1984).

24. F. W. Ostermayer, Jr., P. A. Kohl and R. M. Lum, J. Appl. Phys., 58, 4390 (1985).

25. H. Gerischer and W. Mindt, Electrochim. Acta, 13, 1329 (1968).

26. H. C. Gatos and M. C. Lavine, J. Electrochem. Soc., 107, 427 (1960).

27. P. E. Gregory and W. E. Spicer, Appl. Phys. Lett., 25, 511 (1974).

28. D. N. McFayden, J. Electrochem. Soc., 130, 1934 (1983).

29. C. A. Kavassalis, D. H. Longendorfer, R. A. LeLievre and R. D. Rauh, Mat. Res. Symp. Proc., Wol. 29, 151 (1984).

30. R. D. Rauh and R. A. LeLievre, J. Electrochem. Soc., 132, 2811 (1985).

31. D. V. Podlesnik, H. H. Gilgen and R. M. Osgood, Appl. Phys. Lett., 45, 563 (1984).